Powder Technology 199 (2010) 23–31

Contents lists available at ScienceDirect

Powder Technology

journal homepage: www.elsevier.com/locate/powtec

Multi-scale modeling and control of fluidized beds for the production of solar grade silicon ☆

S. Balaji, Juan Du, C.M. White, B. Erik Ydstie *

Dept. of Chemical Engineering, Carnegie Mellon University, 5000 Forbes Ave, Pittsburgh, PA 15213, USA

ARTICLE INFO

Article history:
Received 25 February 2009
Received in revised form 24 March 2009
Accepted 8 April 2009
Available online 6 June 2009

Keywords:
Multi-scale
Computational fluid dynamics
Chemical vapor deposition
Population balance
Solar grade silicon production

ABSTRACT

In this paper we develop a multi-scale model to describe the growth of silicon particles due to chemical vapor deposition (CVD) in a fluidized bed reactor (FBR). The reactor system is designed to make poly-silicon for solar cell applications by thermal decomposition of silane. The complex interplay between the continuous and the disperse phases and CVD onto the silicon particles in the FBR is modeled using three modules — Computational Fluid Dynamics (CFD), Reaction Module and Population Balance Module (PBM). The Computational Fluid Dynamics (CFD) module describes the hydrodynamics via momentum, mass and heat transfer between different phases. The reaction module describes the homogeneous gas phase reactions and deposition on polycrystalline silicon particles. The population balance represents the dynamic evolution of the particle size distribution. By coupling together the modules, we provide a complete multi-scale model for the particulate CVD process. The resulting nonlinear, multi-scale model is solved using COMSOL Multi-physics and MATLAB. The results from the proposed model match the experimental data obtained from a pilot scale reactor. An inventory controller maintains the void fraction and in turn the average diameter of the silicon particles at the exit.

1. Introduction

Photovoltaic (PV) conversion of solar radiation into electricity is one of the accepted methods which has undergone significant technological and industrial developments recently [1]. While the basic technology for solar energy conversion has changed a little, new processes and improved manufacturing have led to lower cost and higher product consistency. The annual growth (around 30% [21]) of the cumulative capacity of installed PV systems over the past 20 years demonstrates significant industrial and government commitment to photovoltaics.

The cost of producing solar grade (high-purity silicon) feedstock represents around 20% of the total cost of the solar cell production. Most of the existing solar grade silicon production facilities use the well established Siemens process [24] in spite of the fact that its cost reduction potential is limited. Other processes like hot wall decomposition of trichlorosilane, carbothermic reduction of silicon [14,23] and decomposition of silane to silicon powders in free space reactors [26] can give less expensive solar grade silicon but are still in the nascent level. The thermal decomposition of silane (SiH_4) gas to solid silicon in a fluidized bed reactor (FBR) is a viable and cost-effective method [11]. The two major advantages of using FBR are the process is almost isothermal and the solids are well mixed such that a uniform surface treatment and fast deposition are achievable. One disadvantage is that the process is difficult to operate and yield losses may be high.

The feasibility of producing high-purity silicon and fast deposition in a fluidized bed reactor to reduce capital and operating costs has been studied in several laboratory-scale investigations. Hsu et al. [12] identified the factors affecting the size of silicon particles produced in the FBR. They also evaluated reactor performance under various operating conditions. Kojima and Morisawa [17] studied the effect of diluent gases like hydrogen, argon and helium on fines formation, product morphology, crystal growth, and particle size in producing polycrystalline silicon from monosilane. Caussat et al. [8], studied the effect of thermal disturbances and agglomeration phenomena on the reactor performance. They operated the system with smaller particles and observed new phenomena such as changes in fluidization quality caused by silane addition. They also explained the experimental observations through detailed theoretical analysis and using classical FBR models [7].

Apart from the experimental studies, Kimura and Kojima [15] proposed a numerical model of a FBR to study fines formation in polycrystalline silicon production from monosilane. Cadoret et al. [5] applied the computational fluid dynamics code MFIX to simulate the transient state of chemical vapor deposition from silane. 3D simulations were carried out to describe the silane pyrolysis process in a more appropriate way and the results were compared with the 2D simulations. Besides, there are other noteworthy numerical studies on the application of fluidized bed technology for silicon production [18,16,25] as well as numerous patents [19,20]. These efforts provide a solid theoretical foundation for the development of a commercial

☆ Research funded by REC silicon LLC and the National Science Foundation.
* Corresponding author. Tel.: +1 412 268 2235; fax: +1 412 268 7139.
E-mail address: ydstie@cmu.edu (B.E. Ydstie).

0032-5910/$ – see front matter © 2009 Elsevier B.V. All rights reserved.
doi:10.1016/j.powtec.2009.04.022

fluidized bed process. However, a simplified solution strategy with a complete and detailed model which integrates CFD, chemical reaction and population balances for possible use in process scale-up, detailed design and control studies is still missing.

White et al. [27] proposed a population balance model for size distribution of particulate processes using particle mass and number balances over discrete intervals. The novel approach for solving population balance equations proposed in this paper reduces the computation time (relative to the classical approaches like method of moment and discretization using collocation) considerably. White et al. [28] further showed the possibility of coupling population balance with CVD calculations to capture the dynamic particle size distribution. They also proposed a multi-scale approach for accurate modeling of the entire process. In continuation of the above mentioned works by White et al. [27,28], we present the complete multi-scale modeling approach including the effect of computational fluid dynamics along with population balance and chemical vapor deposition models. For the first time in the field of silicon production using FBR, we couple all the effects pertaining to the system (using partial differential equations (CFD), ordinary differential equations (PBM) and algebraic equations (CVD)) and we solve the resulting nonlinear partial differential algebraic equations with a computationally efficient and inexpensive solution methodology.

A multi-scale model is a composite mathematical model formed from two or more submodels that describe phenomena at different scales. It attempts to create flexible and efficient models by linking two or more partial models that describe phenomena at different characteristic length and time scales. This approach provides efficient solutions to problems which cannot be described by uni-scale models [3]. Brandt [3] gives an extensive review of a broad range of multi-scale computational techniques. In the chemical engineering field, there are numerous areas such as crack propagation in a silicon slab [4], fluid behavior in porous media [10] and global climate modeling [22], that require the multi-scale modeling approach. In spite of its major benefits in accurate modeling of a given process, due to the challenges in the integration and pairing of different gradients between different length and time scales, the solution method is still in the developmental stages.

The schematic of the experimental setup and the various phenomena taking place in the reactor is given in Section 2. Details of model development and the solution approach are presented in Section 3. The CFD, CVD and PBM models developed are explained in Sections 4, 5 and 6 respectively. The simulation results from the CFD model followed by the results obtained by combining all the major phenomena in one platform are given in Section 7. Section 8 discusses the inventory control applied to the system along with the sensitivity analysis of important operating variables.

2. Schematic of the experimental setup

The fluidized bed reactor considered in this study is shown in Fig. 1. The silicon seed particles (<1 mm) are fed into the system at rate S. The silane and hydrogen gas (reactants) are fed from the bottom of the reactor. The reactants are fed at the rate of F_{in} to maintain the fluidization and control the residence time to ensure maximum conversion. The feed consists of silane diluted by hydrogen or argon which acts as the fluidization gas. Wall heaters and preheated gas streams are used to heat the fluidized bed to a required reaction temperature. Silicon is produced by thermal decomposition of silane and is deposited on the seed particles. As a result, the silicon seed particles grow in the reactor and are removed from the bottom (product) at rate W. Some of the fine silicon particles (powders) escape the reactor along with hydrogen (F_{out}) at the top exit. The powder production should be minimized to maximize yield. Product particles are withdrawn at a rate such that the solid particle hold up is controlled. Additionally, seed particles are added in such a way that the desired product size distribution is achieved. Thus, the size distribution of the silicon particles at the exit (product) can be controlled by manipulating the reactant flow rate F_{in}, product flow rate W and silicon seed rate S.

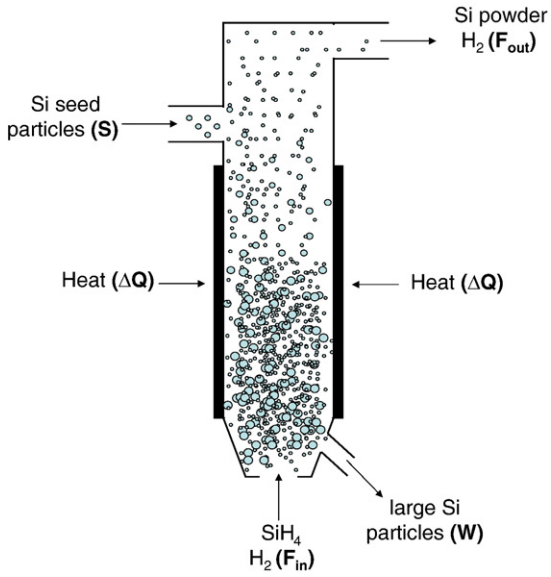

Fig. 1. Fluidized bed reactor.

3. The multi-scale modeling strategy

The reaction between silane and hydrogen is almost instantaneous and the flow and the mixing regimes reach steady state within a few seconds of operation. However, based on the inlet conditions, temperature reaches steady state only after a few minutes. These system level phenomena are captured well by solving the mass, momentum and energy balance equations simultaneously using a two-dimensional heterogeneous model. On the other hand, the micro-level deposition of silicon particles produced in gas phase onto the silicon seed particles is captured by CVD equations. The particle size distribution and the dynamics of the particle growth are represented through particle mass and number balances. This particular dynamics is slow (in the order of hours). Thus, in modeling such a complex system which is characterized by different space and time scales, multi-scale approach is employed as illustrated in this section.

The multi-scale modeling strategy consists of three steps:

Define framework to integrate submodels

In this work, we apply the multi-domain framework [13] where the micro-scale and macro-scale parts occupy adjacent, non-overlapping parts of the system domain. Interface regions exist between domains where both models apply. Micro-scale models define particle nucleation growth and agglomeration which determine the size distribution of particles in the reactor. The macro-scale model represents homogeneous reaction in the gas phase. The micro-scale model is represented by a population balance module while the macro-scale model is represented by a fluid dynamics module. The interface between them is developed by chemical vapor decomposition module which describes particle growth process caused by depositing long chain silicon polymers and scavenging powder produced through homogeneous reaction in the gas phase [18].

Define length scales in each models

Different scales are identified based on the nature of the process and the characteristic length and time scales.

1. Particle scale: The important phenomena are the growth of each particle due to the reaction taking place.

2. Granule scale: Powder formation, granule nucleation, consolidation and coalescence are the main processes at this level.
3. Vessel scale: Temperature, concentration and velocity profile of both the gas and solid phases are crucial at this level.

Develop communication among various modules. The hydrodynamics are modeled using CFD, which provides a basis for a simplified reactor flow model as illustrated in Fig. 2. The kinetic terms and the reactor temperature and concentrations can be expressed as functions of reactor dimensions, void volume and time in the CFD module. Reactor temperature and concentration from the CFD module provide inputs to the CVD module. The CVD module calculates the overall process yield which provides an input to the population balance module. The average particle diameter is then calculated by the population balance module and imported into the CFD module for further calculation. The population balance module and CVD module are solved using MATLAB and the fluid dynamic module is solved using the Multi-physics modeling software COMSOL. The interlink between COMSOL and MATLAB is exploited well to integrate the different modules in a single computational platform (as shown in Fig. 2).

4. The fluid dynamics module

The momentum, mass and energy balance equations are based on multi-phase flows with interphase exchange model [2]. The following assumptions are made:

1. The entire bed can be divided into '*n*' number of zones such that the volume fraction (ε) in each zone is constant. The change in the volume fraction is incorporated in the model calculations by discretizing the entire bed into '*n*' number of zones and specifying the value of (ε) in each zone based on the inlet and outlet velocities of the gas and solid phases in the respective zones. For simplicity, '*n*' is assumed as three in the current study.
2. The particles are spherical and distribute uniformly in each zone of the reactor.

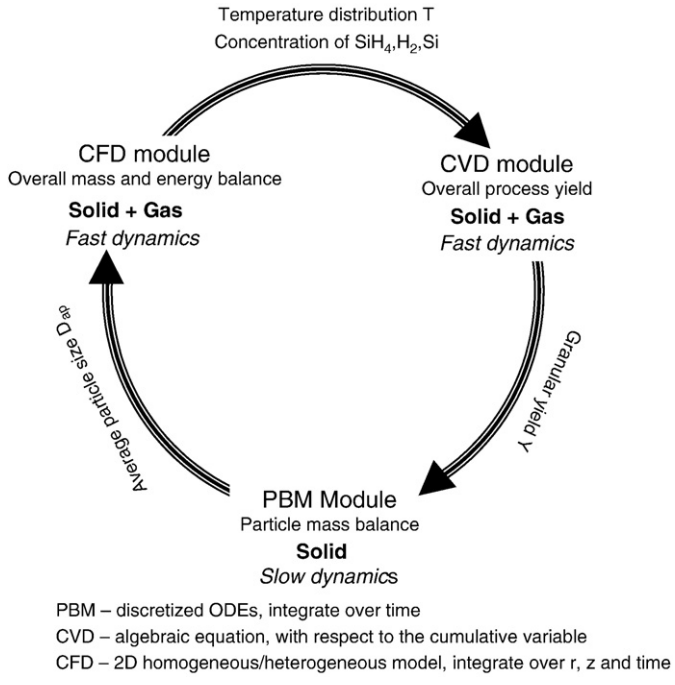

Fig. 2. Multi-scale modeling of the CVD process.

3. Silicon seed particles and their growth are modeled as solid phase and the fine silicon powder formation is compensated as silicon concentrations in gas phase.

Particles inside the fluidized bed reactor are suspended in the reactor due to the balance between the gravity and the drag force caused by the interaction between gas phase and solid phase. Thus the momentum balance for the gas and solid phases is modeled as:

$$\varepsilon_g \frac{\partial}{\partial t}\left(\rho_g \upsilon_g\right) + \varepsilon_g \nabla.\left(\rho_g \upsilon_g \upsilon_g\right) = -\varepsilon_g \nabla.P + \varepsilon_g \rho_g g - F \tag{1}$$

$$\varepsilon_s \frac{\partial}{\partial t}(\rho_s \upsilon_s) + \varepsilon_s \nabla.(\rho_s \upsilon_s \upsilon_s) = -\varepsilon_s \nabla.P + \varepsilon_s \rho_s g + F \tag{2}$$

where ε_g and ε_s are the volume fractions of the gas and solid phases, υ_g and υ_s are the gas and solid phase velocities respectively.

The term F denotes the interface momentum transfer and the effects due to the appearance and/or disappearance of chemical species in gas and solid phases. In this case, silicon in the gas phase deposits on the silicon particles (solid phase). Therefore, it is necessary to include the rate of production effects in solid phase. However, the effect of particle growth and the corresponding changes in the particle diameter is calculated in the CVD and PBM calculations. This information is updated continuously into the CFD model equations. Hence the second term in Eq. (3) can be neglected.

$$F = -\beta_{gs}\left(\upsilon_g - \upsilon_s\right) + R_{gs}\left(\xi_{gs}\upsilon_s + \overline{\xi}_{gs}\upsilon_g\right). \tag{3}$$

The drag coefficient between the gas and the solid phases β_{gs} is given by

$$\beta_{gs} = \frac{3\varepsilon_s\varepsilon_g\rho_g}{4V_{rs}^2 d_p}\left(0.63 + 4.8\sqrt{V_{rs}/Re_s}\right)^2 |\upsilon_g - \upsilon_s|. \tag{4}$$

R_{gs} is the total reaction rate between the two phases. Further details about the balance equations can be obtained from Benyahia et al. [2].

The mass balance equation is given by:

$$\varepsilon_g \frac{\partial}{\partial t}(c_i) + \varepsilon_g \nabla.\left(\upsilon_g c_i\right) = \nabla.\left(D_{eff,i}\frac{\partial c_i}{\partial x}\right) + R_i \tag{5}$$

where $i = SiH_4$, Si, H_2. D_{eff} is the effective diffusivity, R_i is the rate of reaction of species i and c_i is the concentration of species i.

The energy balance equation for the solid and gas phases is written as:

$$\varepsilon_s \frac{\partial}{\partial t}\left(\rho_s C_{ps} T_s\right) + \varepsilon_s \nabla.\left(\upsilon_s \rho_s C_{ps} T_s\right) = \varepsilon_s \nabla.\left(k_s \frac{\partial T_s}{\partial x}\right) + Q_s - \gamma_{gs}\left(T_s - T_g\right) \tag{6}$$

$$\varepsilon_g \frac{\partial}{\partial t}\left(\rho_g C_{pg} T_g\right) + \varepsilon_g \nabla.\left(\upsilon_g \rho_g C_{pg} T_g\right) = \varepsilon_g \nabla.\left(k_g \frac{\partial T_g}{\partial x}\right) + Q_g + \gamma_{gs}\left(T_s - T_g\right) \tag{7}$$

where C_{pi} is the heat capacity of species i, k_i is the thermal conductivity of i and Q_i represents the heat produced or utilized. γ_{gs} denotes the heat transfer coefficient between the two phases and is calculated by

$$\gamma_{gs} = \frac{6k_g\varepsilon_s Nu_s}{d_p^2}. \tag{8}$$

The volume fractions of the gas and solid phases are related as:

$$\varepsilon_g + \varepsilon_s = 1. \tag{9}$$

The expressions for rate of reaction used in this work [27] are:

homogeneous reaction rate

$$R_{\text{hom}} = 2e13 \exp\left(\frac{-26,000}{T_g}\right) c_{SiH_4} \tag{10}$$

heterogeneous reaction rate [27]:

$$R_{\text{het}} = 2.79e8 \exp\left(\frac{-19,530}{T_s}\right) c_{SiH_4}. \tag{11}$$

The heterogeneous reaction rate does not play a significant role under the experimental conditions reported here and hence not included in the calculations.

5. The reaction module

Silicon particles in the reactor grow by scavenging [18] a fraction of silicon polymers and powder produced through homogeneous decomposition according to Eq. (10). The reaction model is developed based on the scavenging factor which determines the fraction of powder deposited on the particles. We assume that the rate of powder scavenging is proportional to the concentration of silicon powder produced by homogeneous reaction and to the total surface area of the silicon particles [27]. In general, the total granular yield is the combination of the heterogeneous reaction and the powder scavenged by the particles. In this application, we just consider the powder scavenged by the particles as heterogeneous reaction is less significant. We then calculate the granular yield as a function of reactor height and integrate, such that:

$$Recovery = Y / M_{\text{in}} \tag{12}$$

$$Y = R_{\text{het}(x)} * V_g + R_{\text{sc}} \tag{13}$$

$$V_g = V_t - V_s \tag{14}$$

$$V_s = M_{\text{Si}} / \rho_{\text{Si}} \tag{15}$$

$$R_{\text{sc}} = k_{\text{sc}} * c_{\text{powder}} \tag{16}$$

$$M_{\text{in}} = c_{\text{in}} * \upsilon_{\text{in}} * A_{\text{reactor}} \tag{17}$$

where n is the total number of particles, M_{Si} is the total mass of silicon. M_{in} is the inlet flow rate of silicon, c_{in} is the inlet silane concentration and υ_{in} is the gas inlet velocity. $A_{reactor}$ is the cross sectional area of the reactor. In Eq. (13), $R_{het(x)}$ is considered as zero.

6. The population balance module

A discrete population balance model is used to understand and predict the size distribution achieved during production. Fig. 3 illustrates the modeling technique applied to particles in a fluid bed system. The analysis assumes that particles are distributed among N size intervals characterized by an average number of moles (or mass) per particle, m_i. Deposition onto the particles causes them to grow from one size interval to the next. The material transfer from the precursor to the particle substrate is represented by r_i, while the flow of particles from one size interval to the next, caused by growth, is represented by f_i. The term q_i represents the addition of seed particles or the withdrawal of product. It is also possible to account for particle aggregation or breakage. The terms fa_i^{in} and fa_i^{out} represent particle movement to and from interval i due to aggregation. The resulting molar balance over a size interval can then be represented as

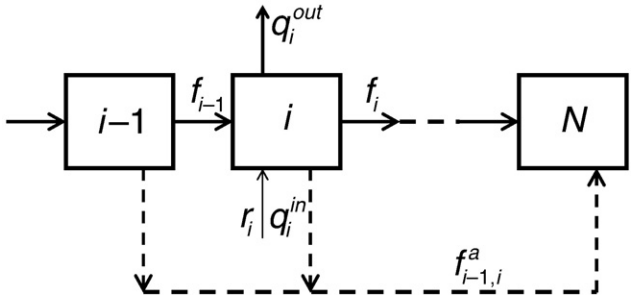

Fig. 3. Size interval characterization of particles.

$$\frac{dM_i}{dt} = f_{i-1} + r_i - f_i + fa_i^{in} - fa_i^{out} + \sum_{\gamma} q_{i,\gamma}, \tag{18}$$

where M_i is the number of moles of particles in an interval. We obtain the total rate of deposition (Y) from the reaction module and the distribution to particles is proportional to the available surface area. Therefore,

$$r_i = Y \cdot \frac{A_i}{\sum_{i=1}^{N} A_i}. \tag{19}$$

We also assume that the particle flow rates to and from the system (q_i) are known or controlled. The flow that results from aggregation has the form $fa_{i,j} = k_{i,j} C_i C_j$, which indicates that the extent of aggregation is proportional to the product of concentrations of aggregating particles. The proportionality constant $k_{i,j}$ can be determined empirically. The flow in and out of interval i due to aggregation is

$$fa_i^{in} = \sum_j \sum_k fa_{j,k}, \text{ for } m_i^{LB} \le \left(m_j + m_k\right) < m_{i+1}^{LB} \tag{20}$$

$$fa_i^{out} = \sum_j \left(fa_{i,j} \cdot \frac{m_i}{m_i + m_j} \right). \tag{21}$$

m_i^{LB} represents the lower bound on the mass of particles in interval i. Under the assumptions that the average particle size in an interval (m_i) is constant and the number of particles is a continuous parameter, particle number balance can be written to obtain the molar flow between the two size intervals. That is,

$$f_i = r_i \cdot \frac{m_{i+1}}{m_{i+1} - m_i}. \tag{22}$$

The population balance module is based on the assumption that the particle phase is well mixed on the time scale of particle growth (several hours). This assumption has been verified in a separate study on the flow of particles using a Fluent based 3D model of the fluidization. Further details can be obtained from Chapalamadugu [9].

7. Results and discussion

7.1. CFD results

Unsteady state 3D simulations for the FBR were carried out using Fluent [9]. The height of the fluidized bed in these simulations was 7 m and the diameter of the reactor body was 0.5 m. An example of such a simulation is shown in Fig. 4. Silicon particles with a diameter of 0.5 mm were filled in the reactor to a height of 3.6 m initially as shown in the figure indicated by the letter (A). No reaction or particle growth takes place and the particles are assumed to be uniform spherical particles. The unsteady state simulations showed that uniform fluidization was achieved very quickly and that the particle phase was well mixed at the time scale of particle growth.

The operating conditions used for the current simulation are given in the Appendix. Simulation and experiments show that the volume

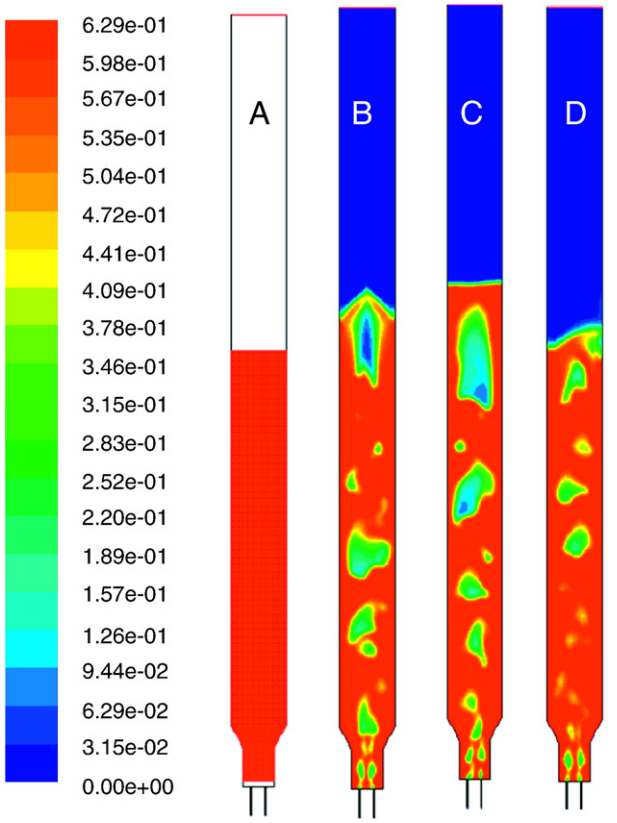

Fig. 4. Unsteady state simulation of the fluidized bed reactor. A at 0 s, B at 3.61 s, C at 5.01 s, and D at 9.22 s.

fraction within the bed varies quite significantly. However, the change in the void fraction for a given set of input condition reaches steady state within a few time steps. Thus, the void fraction along the bed is not solved explicitly. Instead, to capture the spatial variations, the entire bed is divided into three zones and the volume fraction in each zone is assumed to be constant. The region just above the introduction of seed particles is considered as one zone and the region below it (fluidized with silicon particles) is divided into two equal zones. The values assumed are based on the void fraction profiles given in Chapalamadugu [9] and Cadoret et al. [6]. The number of zones can be increased further with appropriate void fraction values to obtain accurate results.

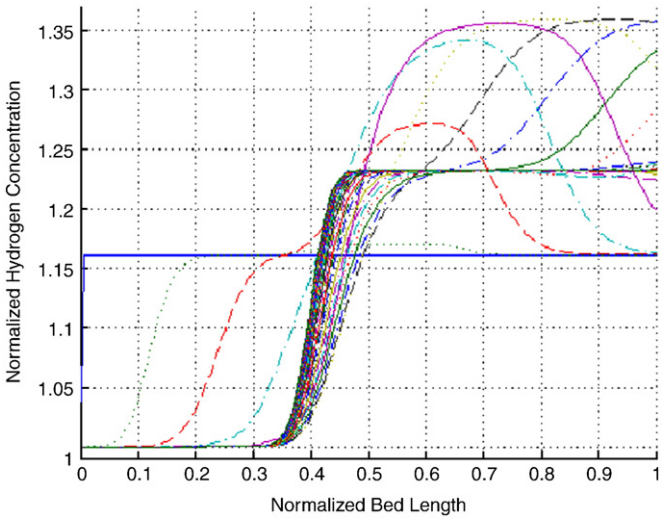

Fig. 6. Dynamics of the normalized hydrogen concentration along the reactor.

Fig. 5 shows the concentration of silane along the reactor during various time intervals. Similarly, hydrogen and silicon produced due to the silane decomposition is shown in Figs. 6 and 7 respectively. From the results obtained, it can be inferred that most of the reaction takes place at the center, as the reactor is heated above ignition temperature at the center.

Fig. 6 shows that the hydrogen produced initially is more than the hydrogen produced at the steady state. This is because of the initial condition chosen. Some amount of silane and hydrogen is assumed to be present in the reactor at time $t=0$. Thus, more hydrogen is seen at the downstream region (bottom of the reactor) due to the initial decomposition of silane along with the initial hydrogen concentration throughout the reactor. This is evident from the concentration profiles of silane at intermediate time steps (before reaching steady state) in Fig. 5.

The concentration and temperature profiles (Figs. 5–9), show that steady state reaches within a few time steps (30 s) which agrees with the assumption that we made in developing the multi-scale modeling strategy. Various profiles shown in the figures are recorded at different and varying time instances to capture the dynamics of the system appropriately. Fig. 9 shows the temperature of the seed silicon particles. It shows that the solid phase temperature is high enough to promote reaction only for a portion of the reactor starting from the inlet port of the silicon seed particles. Note that the model equations for the silicon

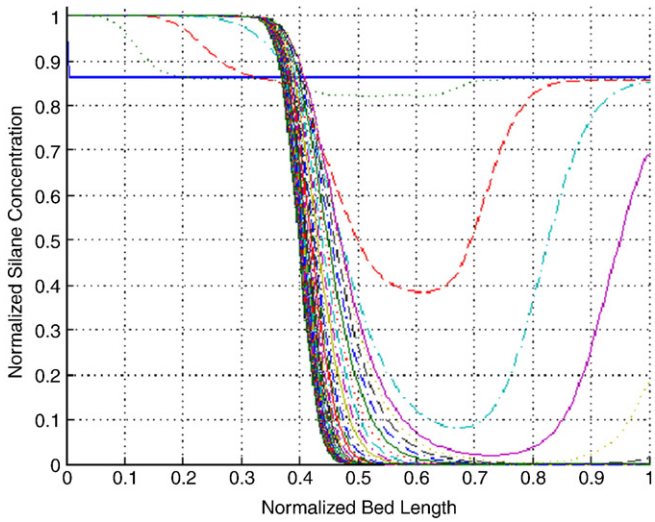

Fig. 5. Dynamics of the normalized silane concentration along the reactor.

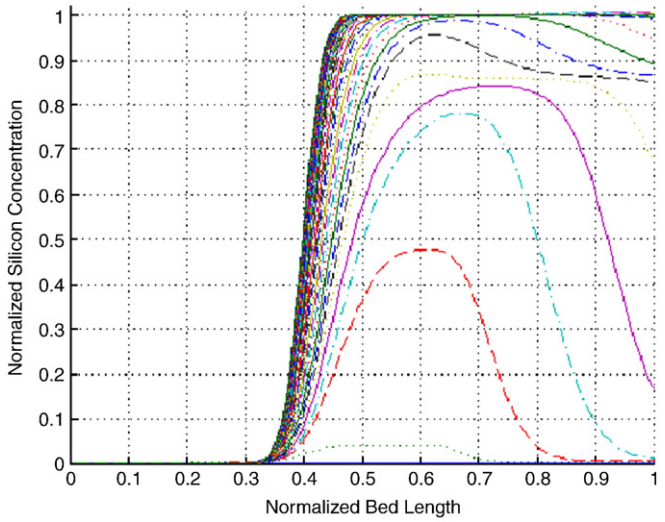

Fig. 7. Dynamics of the normalized silicon concentration along the reactor.

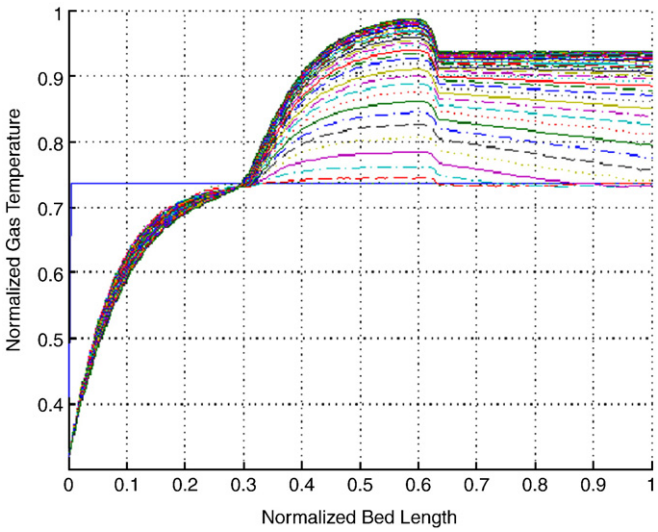

Fig. 8. Dynamics of the normalized gas temperature along the reactor.

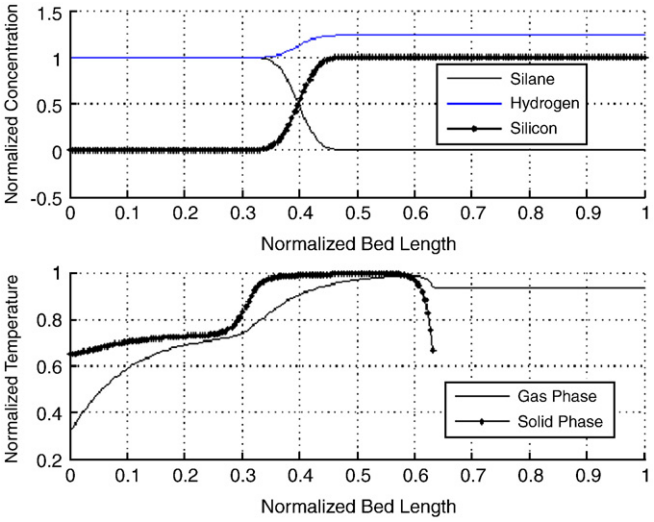

Fig. 10. Steady state profiles along the reactor.

particles are valid only from the point where the seed particles enter the reactor. However, the gas phase is solved for the entire reactor. This explains the difference in the normalized lengths along the *x*-axis in Figs. 8 and 9. From Fig. 9, it is seen that the seed particles enter the reactor at a relatively low temperature and get heated up due to the heat exchange between the gas and the solid particles. The steady state profiles for concentration and temperature are shown separately in Fig. 10. The profiles are dependent on the void fractions assumed in each zones. Thus, the void fraction values and the length of each zone are to be changed based on the operating conditions. The simulations are carried out with fixed operating conditions based on the experimental data. A relation between the spatial variations in the void fraction and the operating variables can be developed both theoretically and using data analysis, and can be implemented directly into the model equations. However, our focus is to devise a multi-scale model connecting various phenomena in one platform. Hence, the void fraction values are assumed as constants in the present study.

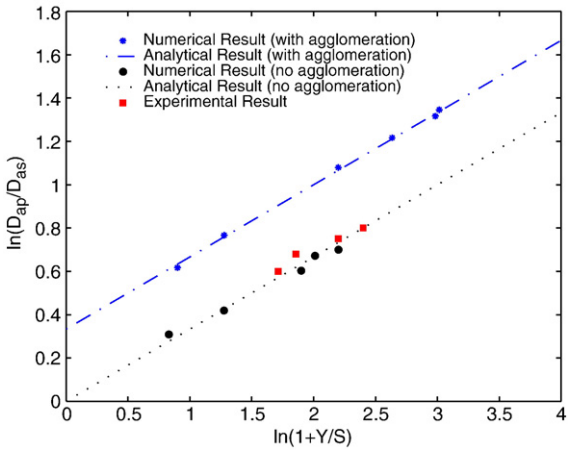

Fig. 11. Model validation.

7.2. Multi-scale modeling results

The results obtained by coupling all the mechanisms based on the multi-scale approach (Fig. 2) are discussed in this section. In Fig. 11, we compare the numerical results with the analytical and the experimental results. As per the experiments conducted at REC Inc., the agglomeration of particles does exist to a certain extent and hence the phenomena of agglomeration are included in the proposed model. The

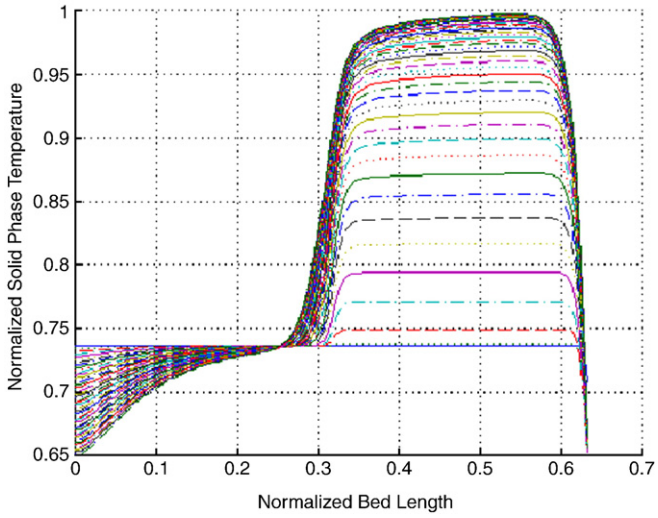

Fig. 9. Dynamics of the normalized solid phase temperature along the reactor.

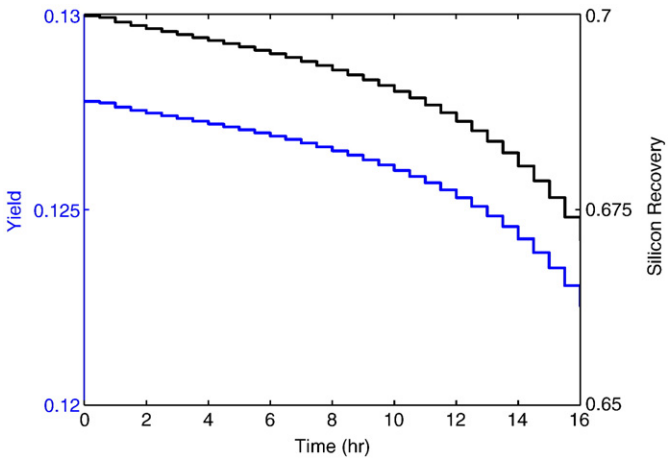

Fig. 12. Total yield and the percentage recovery of silicon determined using the multi-scale modeling approach for a batch experiment.

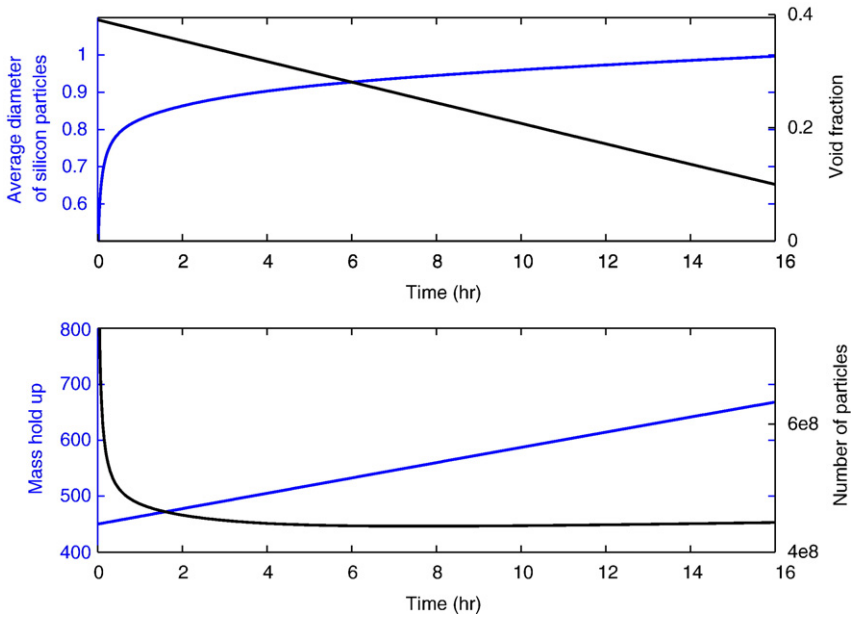

Fig. 13. Effect of mass hold up or the product flow rate on the important parameters of the system.

analytical expressions are obtained from [28]. The relationship between process flow rates and average particle size is given by

$$1 + \frac{W}{S} = \frac{n_p}{n_s}\left(\frac{D_{ap}}{D_{as}}\right)^3 \tag{23}$$

where W is the product flow rate and S is the seed flow rate. D_{ap} is the average particle diameter of product and D_{as} is the average particle diameter of seed. n_p is the number of particles withdrawn and n_s is the number of particles added.

If $\ln(1+W/S) = 3\ln(D_{ap}/D_{as})$ holds good based on the experimental data, then from Eq. (23), $n_p/n_s = 1$. This infers that there is no nucleation, agglomeration, or breakage. On the other hand, $n_p/n_s < 1$, indicating that there is particle agglomeration in the reactor. Further details on the analytical results can be obtained from White et al. [28]. From the results obtained (Fig. 11), the numerical results follow the same trend as the analytical and experimental results and hence the proposed multi-scale model can be used for further studies.

Fig. 12 shows the total yield of silicon obtained from the reactor and the corresponding recovery. In the model equations, the amount of silicon particles to be removed from the system to maintain the void fraction and the extent of reaction in the reactor is unknown. Hence, the simulations are carried out such that the product withdrawal rate is much smaller than the seed flow rate. These simulations are carried out to study the effect of void fraction and mass hold up on the average diameter of the particles. From the figure, we infer that void fraction decreases as silicon hold up increases, resulting in a decrease in the overall yield of the process. Fig. 13 shows that as mass hold up increases, the void fraction slowly decreases leading to a decrease in the overall yield and recovery (Fig. 12). However, there is an increase

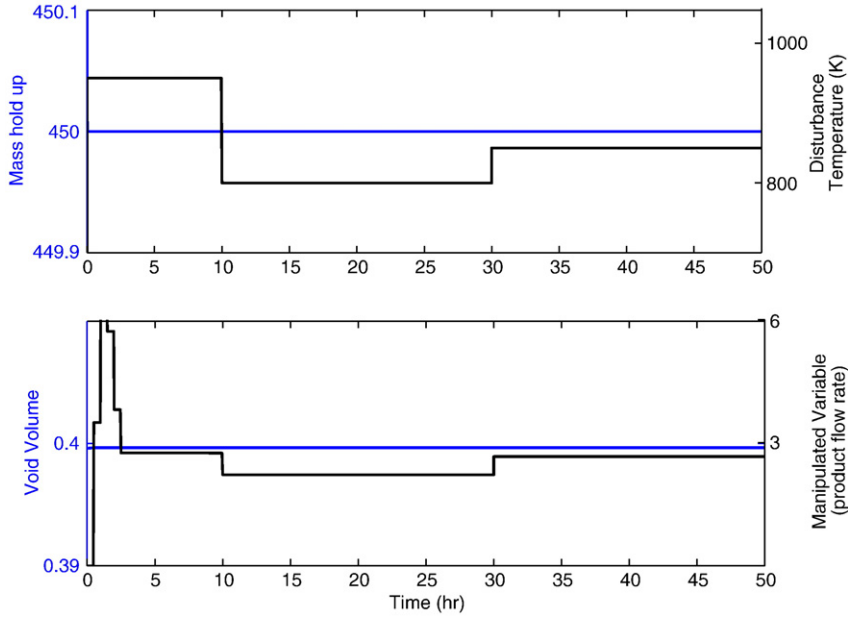

Fig. 14. Closed loop simulation results.

in the average diameter of the silicon particles. Thus, the mass hold up and in turn the product flow rate should be maintained in such a way that the desired particle size can be obtained.

7.3. Inventory control

The above discussion demonstrates that controlling the product flow rate is crucial to obtain stability and the desired performance of the FBR system for making solar grade silicon. We achieve this objective using inventory control based on the overall mass of the system [28]. An inventory control strategy for the silicon mass hold up can be written as:

$$\frac{dM}{dt} = -K(M - M^*) \tag{24}$$

where K is the proportionality constant, M is the mass hold up and M^* is the set point. The mass balance equation for silicon is:

$$\frac{dM}{dt} = S + Y - W \tag{25}$$

where S is the seed flow rate, Y is the amount of silicon produced and W is the product flow rate. The product flow rate can be manipulated to keep the mass hold up to a specified value M^* using:

$$W = S + Y + K(M - M^*). \tag{26}$$

The simulated results show that the void fraction or the mass hold up can be controlled with the proposed strategy by manipulating the product flow rate and furthermore, the system converges to the steady state. The controller is also tested with a few disturbances in the system. The heat input to the system or the reactants flow rates are assumed as disturbance variables. The controller performs well with a significant disturbance in the process variables (Fig. 14).

7.4. Closed loop sensitivity analysis

A closed loop sensitivity analysis for the process based on the multi-scale model is discussed in this section. Steady state simulations are carried out to determine the effect of important parameters like bed temperature (T_b) and the scavenging coefficient k_{sc}. The results obtained are tabulated in Tables 1–4. The results show that the granular yield is highly dependent on k_{sc}. With increasing k_{sc}, more silicon powders produced due to the reaction are scavenged and deposited on the silicon seed particles. Thus, with increasing k_{sc}, the silicon is produced and the recovery is increased.

Similarly, with increase in the bed temperature, the reaction rate increases. This results in silane decomposition at early stages in the reactor, increasing the time for scavenging the silicon powders onto the seed particles. Thus, with an increase in the bed temperature, the recovery also increases. Therefore, the temperature needs to be controlled to obtain a desired performance for the process.

Table 1
Multi-scale modeling results with $k_{sc} = 0.0013$.

T_b (K)	k_{sc}	Y_{total} (mol/s)	Recovery
960	0.0013	0.1665	0.9119
920	0.0013	0.1639	0.8978
880	0.0013	0.1544	0.8457
840	0.0013	0.1182	0.6475

Table 2
Multi-scale modeling results with $k_{sc} = 0.0010$.

T_b (K)	k_{sc}	Y_{total} (mol/s)	Recovery
960	0.001	0.1281	0.7014
920	0.001	0.1261	0.6906
880	0.001	0.1188	0.6505
840	0.001	0.0909	0.4981

Table 3
Multi-scale modeling results with $k_{sc} = 0.0007$.

T_b (K)	k_{sc}	Y_{total} (mol/s)	Recovery
960	0.0007	0.0896	0.4910
920	0.0007	0.0883	0.4834
880	0.0007	0.0831	0.4554
840	0.0007	0.0637	0.3486

Table 4
Multi-scale modeling results with $k_{sc} = 0.0005$.

T_b (K)	k_{sc}	Y_{total} (mol/s)	Recovery
960	0.0005	0.0640	0.3507
920	0.0005	0.0630	0.3453
880	0.0005	0.0594	0.3253
840	0.0005	0.0455	0.2490

8. Conclusions

In this paper, a comprehensive multi-scale model is implemented to describe the growth of silicon particles in a fluidized bed reactor. The proposed model incorporates hydrodynamic, momentum exchange, mass and heat transfer and kinetic rate to describe both heterogeneous and homogeneous reactions. Population balance is used to represent the growth and aggregation of silicon particles. The simulations are successfully carried out and validated against the experimental and analytical results. The model contains an adjustable parameter called scavenging factor to predict the silicon yield. Apart from the modeling efforts, an inventory based control is implemented to control the overall mass hold up of the system and a closed loop sensitivity analysis is carried out based on temperature and scavenging factor.

The particle diameter at the exit (product) is not only dependent on the void fraction. It is a strong function of silicon seed flow rate and the inlet flow rates of silane and the temperature prevailing in the system. Thus, a comprehensive inventory control based on the overall mass and the overall energy of the system is necessary to complete the control study. The emphasis of the current work is to devise a model with control view point. A detailed study on developing a control strategy or framework for this system will be dealt in the future.

Appendix

The drag coefficient between the gas and the solid phases is calculated using Eq. (4). The term V_{rs} is determined [2] based on

$$V_{rs} = 0.5(A - 0.06Re_s) + \sqrt{0.06Re_s^2 + 0.12Re_s(2B - A) + A^2}$$

$$A = \epsilon_g^{4.14}$$

$$B = 0.8\epsilon_g^{1.28}$$

$$Re_s = \frac{d_p|v_g - v_s|\rho_g}{\mu_g}.$$

The mass transfer coefficient γ_{gs} is determined using Eq. (8). The Nusselt number is

$$Nu_s = \left(7 - 10\varepsilon_g + 5\varepsilon_g^2\right)\left(1 + 0.7Re_s^{0.2}Pr^{1/3}\right) + \left(1.33 - 2.4\varepsilon_g + 1.2\varepsilon_g^2\right)Re_s^{0.7}Pr^{1/3}.$$

Boundary conditions employed in the simulation are obtained from White et al. [27]:

Inlet velocity of silane gas: 0.55 m/s
Temperature of inlet gas: 300 K
Concentration of silane: 6.5 mol/m^3
Concentration of hydrogen: 56 mol/m^3
Concentration of silicon powder: 0.001 mol/m^3
Inlet velocity of seed particles: 1e−3 m/s.

References

[1] I.A. Abba, J.R. Grace, Spanning the flow regimes: generic fluidized bed reactor model, AIChE Journal 49 (2003) 1838–1848.
[2] S. Benyahia, M. Syamlal, T.J. O'Brien, Summary of MFIX Equations 2005-4, U.S Department of Energy, 2006.
[3] A. Brandt, Multi-scale and Multi-resolution Methods: Theory and Applications, Springer, 2002.
[4] J. Broughton, F. Abraham, N. Bernstein, E. Kaxiras, Concurrent coupling of length scales: methodology and application, Physical Review, B 60 (4) (1999) 2391–2403.
[5] L. Cadoret, N. Reuge, S. Pannala, M. Syamlal, C. Coufort, B. Caussat, Silicon CVD on powders in fluidized bed: experimental and multi-fluid Eulerian modelling study, Surface and Coatings Technology 201 (2007).
[6] L. Cadoret, N. Reuge, S. Pannala, M. Syamlal, C. Rossignol, J. Dexpert Ghys, C. Coufort, B. Caussat, Silicon chemical vapor deposition on macro and submicron powders in a fluidized bed, Powder Technology 190 (2009) 185–191.
[7] B. Caussat, M. Hemati, J.P. Couderc, Silicon deposition from silane or disilane in a fluidized bed—part ii: theoretical analysis and modeling, Chemical Engineering Science 50 (22) (1995) 3625–3635.
[8] B. Caussat, M. Hemati, J.P. Couderc, Silicon deposition from silane or disilane in a fluidized bed—part i: experimental study, Chemical Engineering Science 50 (22) (1995) 3615–3624.
[9] V.V.R. Chapalamadugu. Dynamic modeling of gasifier for integrated gasification combined cycle. MS Thesis, Carnegie Mellon University, Pittsburgh PA., 2007.
[10] J. Cushman, Theory and Applications of Transport in Porous Media, Kluwer Academic Publishers, Dordrecht, 1997.
[11] T. Furusawa, T. Kojima, H. Hiroha, Chemical vapor deposition and homogeneous nucleation in monosilane pyrolysis within interparticle spaces — application of fines formation analysis to fluidized bed CVD, Chemical Engineering Science 43 (1988) 2037–2042.
[12] G. Hsu, N. Rohatgi, J. Houseman, Silicon particle growth in a fluidized bed reactor, AIChE Journal 33 (5) (1987) 784–791.
[13] G.D. Ingram, I.T. Cameron, K. M Hangos, Classification and analysis of integrating frameworks in multi-scale modelling, Chemical Engineering Science 59 (2004) 2171–2187.
[14] S.M. Karabanov, New technologies for solar grade silicon production, Materials Research Society Symposium Proceedings 716 (2002) B11.8.1–B11.8.5.
[15] T. Kimura, T. Kojima, Numerical model of a fluidized bed reactor for polycrystalline silicon production-estimation of CVD and fines formation, Journal de Physique IV 2 (1991) C2:103-C2:110.
[16] T. Kojima, T. Kimura, M. Matsukata, Development of numerical model for reactions in fluidized bed grid zone: application to chemical vapor deposition of polycrystalline silicon by monosilane pyrolysis, Chemical Engineering Science 45 (1990) 2527–2534.
[17] T. Kojima, O. Morisawa, Production of polycrystalline silicon from monosilane in a fluidized bed — effects of the diluent gas on the conversion and on the properties of the product, International Chemical Engineering 32 (4) (1992) 767–775.
[18] S. Lai, M.P. Dudukovic, P.A. Ramachandran, Chemical vapor deposition and homogeneous nucleation in fluidized bed reactors: silicon from silane, Chemical Engineering Science 41 (1986) 633–641.
[19] S. Lord and R. Milligan, editors. Method for silicon deposition. U.S. Patent 5798137.
[20] S. Lord and R. Milligan, editors. Silicon deposition reactor apparatus. U.S. Patent 5810934.
[21] A. Luque, S. Hegedus (Eds.), Handbook of Photovoltaic Science and Engineering, John Wiley & Sons, 2003.
[22] M. Mayer, C. Wang, M. Webster, R. Prinn, Linking local air pollution to global chemistry and climate, Journal of Geophysical Research—Atmospheres 105 (D18) (2000) 22869–22896.
[23] J.P. Murray, G. Flamant, C.J. Roos, Silicon and solar-grade silicon production by solar dissociation of Si_3N_4, Solar Energy 80 (10) (2006) 1349–1354.
[24] W.C.O Mara, R.B. Herring, I.P. Hunt (Eds.), Handbook of Semiconductor Silicon Technology, Noyes Publications, Park Ridge, NJ, 1990.
[25] J. Pina, V. Bucala, N. Schbib, P. Ege, H.I. de Lasa, Modeling a silicon CVD spouted bed pilot plant reactor, International Journal of Chemical Reacor Engineering 4 (A9) (2006).
[26] T. Sill, R. Sonnenschein, A. Muller, A. Golz, C. Beyer, P. Adler, New process for cost effective solar silicon from monosilane, Proceedings of the 21st European Photovoltaic Solar Energy Conference, 2006.
[27] C.M. White, P. Ege, B.E. Ydstie, Size distribution modeling for fluidized bed solar-grade silicon production, Powder Technology 163 (2006) 51–58.
[28] C.M. White, G. Zeininger, P. Ege, B.E. Ydstie, Multi-scale modeling and constrained sensitivity analysis of particulate CVD systems, Chemical Vapor Deposition 13 (2007) 507–512.

Glossary

A_i: surface area of average particle; m^2
$A_{reactor}$: cross sectional area of reactor; m^2
c: concentration; mol/m^3
C_p: heat capacity; J/kg· K
d_p: diamaeter of particles; m
D_a: average particle diameter; m
D_{eff}: effective diffusivity; m^2/s
f: particle flow between size intervals; mol/s
fa: particle flow due to aggregation; mol/s
F: interface momentum transfer; N/m^3
F_{in}: gas inlet flow rate; mol/s
F_{out}: gas outlet flow rate; mol/s
g: acceleration due to gravity; m/s^2
k: thermal conductivity; W/m· K
$k_{i,j}$: aggregation proportionality constant; m^6/(mol. s)
k_{sc}: scavenging factor; m^3/s
K: controller gain; 1/s
m_i: number of moles in average particle of size interval; mol
M_i: total moles of silicon in size interval i; mol
M_{in}: inlet flow rate of silane; mol/s
M_{Si}: total mass of silicon insider reactor; kg
n: number of particles
Nu: Nusselt number
Pr: Prandtl number
q: external particle flow; mol/s
Q: heat produced or consumed; W/m^3
r: silicon production in size interval; mol/s
R: reaction rate; mol/m^3· s
Re: Reynolds number
S: silicon seed inlet flow rate; mol/s
t: time; s
T: temperature; K
v: velocity; m/s
V: volume; m^3
W: silicon product withdrawal rate; mol/s
Y: silicon production rate; mol/s
ε: volume fraction
ρ: density; kg/m^3
γ: heat transfer coefficient; J/m^3· K ·s
β: drag coefficient; kg/m^3· s

Subscripts

g: gas phase;
s: solid phase;
gs: gas–solid interface;
i: species or size interval;
tot: total;
het: heterogeneous;
hom: homogeneous;